

## Reduced Representations of Vector-Valued Coupling Variables in Decomposition-Based Design Optimization

**Michael J. Alexander<sup>1</sup>, James T. Allison<sup>2</sup>, Panos Y. Papalambros<sup>3</sup>**

<sup>1</sup> University of Michigan, Ann Arbor, Michigan, U.S.A., malexanz@umich.edu

<sup>2</sup> The MathWorks, Natick, Massachusetts, U.S.A., james.allison@mathworks.com

<sup>3</sup> University of Michigan, Ann Arbor, Michigan, U.S.A., pyp@umich.edu

### 1. Abstract

Decomposition-based methods for system design optimization introduce consistency constraints, which contain coupling variables communicated between adjacent subproblems and link them together. When these variables are vector-valued (e.g., dynamic responses), the problem size can increase dramatically and make such methods impractical. Therefore, it is necessary to represent these vector-valued coupling variables with a reduced representation that will enable efficient optimization while maintaining an acceptable level of accuracy with respect to the original representation. This study investigates two representation techniques, radial-basis function artificial neural networks and proper orthogonal decomposition, and implements each in an analytical target cascading problem formulation for electric vehicle powertrain system optimization. Implementation of each representation technique is demonstrated and the techniques are assessed in terms of efficiency (decision vector dimensionality) and accuracy.

**2. Keywords:** Decomposition-based design optimization, analytical target cascading, coupling variables, reduced representation, vector-valued target.

### 3. Introduction

In formulating design optimization problems for large-scale, complex systems, it is often practical to separate these systems into simpler, more manageable subsystem configurations. Decomposition-based optimization strategies are used frequently to solve these problems. These strategies introduce consistency constraints [1], which contain coupling variables and ensure feasible design solutions. Coupling variables appear in subproblem optimization formulations as decision variables, increasing subproblem dimension. If these coupling variables consist of a small, finite number of scalars, problem size does not increase appreciably, and efficient optimization of the system is still possible. However, if coupling comprises infinite-dimensional variables, such as functions, ensuring consistency becomes computationally challenging. Discretization is typically applied, transforming infinite-dimensional variables into finite-dimensional ones, which can be represented in vector form as

$$f(y) = [f(y_1), f(y_2), \dots, f(y_q)]^T = [f_1, f_2, \dots, f_q]^T, \quad (1)$$

where  $y$  is the independent variable and  $q$  is the number of discretized points. Although this transformation enables consistency constraints to be computed, it requires a large number of discretization points to ensure a sufficiently accurate representation of the function. The dimensionality (measured by  $q$ ) of these vector-valued coupling variables (VVCVs) can become very large, resulting in high-dimension subproblem decision vectors. Thus, it is desirable to approximate VVCVs with a reduced dimension representation that preserves sufficient accuracy. The new coupling variables comprising these representations are known as reduced representation variables [2].

With the exception of the work by Sobieski [3], published literature has not addressed this issue. The majority of published techniques use simplified models of objective functions and constraints to approximate their more computationally-expensive counterparts. These methods, classified broadly as metamodeling ones [4], have a similar motivation as the problem at hand in that both approaches attempt to represent functions more efficiently under a sufficient level of accuracy. The difference, however, is that metamodeling focuses on efficiency in terms of computational expense, whereas the reduced representations here focus on efficiency in terms of decision vector dimensionality during optimization. With this motivation, one can explore alternatives beyond the traditional metamodeling techniques.

The particular motivating application is the use of analytical target cascading (ATC) for hybrid-electric vehicle (HEV) powertrain system optimization. In early unpublished work on this problem, it was necessary to reduce the representation of VVCVs associated with maximum motor/generator torque curves and power loss maps. Polynomial interpolation [5] and polynomial response surface (PRS) approximation [6-8] were initially implemented, with the polynomial coefficients serving as reduced representation variables. However, these

methods were deemed ineffective as many coefficients were required to produce approximations of reasonable accuracy. In a more heuristic approach, weighting coefficients were used as reduced representation variables in the linear interpolation of two distinct “baseline” functions to approximate the original representations. While this technique significantly reduced the size of VVCVs, the accuracy of the new representations was significantly compromised. Image warping [10, 11], which used warping parameters as reduced representation variables, also demonstrated some efficacy but it was challenging to determine appropriate transformations for the motor curve and map. In an earlier, related ATC study [12], it was observed that implementing radial-basis function (RBF) artificial neural networks (ANN) [13, 14] with input variables serving as reduced representation variables was a promising approach.

Another promising approach coming from data analysis is proper orthogonal decomposition (POD) [15, 16]. POD is based on principal component analysis (PCA) [17, 18] and can be used for state-space reduction of dynamical systems. POD emerged as an interesting candidate for further study because it employs concepts similar to linearly combining orthogonal functions, with the advantage that the orthogonal functions in POD are based on formal, mathematical techniques that ensure orthogonality [19, 20].

This paper examines the implementation of RBF ANN and POD in the optimization of an electric vehicle powertrain system using ATC. Section 4 reviews ATC briefly; Section 5 discusses the reduced representations using RBF ANN and POD; Section 6 presents a summary of the vehicle model; Sections 7 and 8 present results and their assessment, respectively; and Section 9 offers some conclusions.

#### 4. Review of Analytical Target Cascading

ATC is a decomposition-based optimization strategy applied to large-scale systems that uses a hierarchical structure to enable design targets determined at upper levels to be cascaded down to lower levels. This technique then attempts to minimize deviations between design targets and subsystem responses to achieve an optimal solution for the system [21, 22].

The system is first decomposed into subproblems hierarchically. In this configuration, the top level is known as the system level and the lower levels are known as subsystem levels. Additionally, a subproblem linked above any given element of interest is known as a parent and those subproblems linked below a given element of interest are known as children. The general ATC subproblem  $P_{ij}$  for the  $i$ th level and  $j$ th element can be defined as [1]:

$$\begin{aligned} & \min_{\bar{\mathbf{x}}_{ij}} f_{ij}(\bar{\mathbf{x}}_{ij}) + \pi(\mathbf{c}(\bar{\mathbf{x}}_{11}, \dots, \bar{\mathbf{x}}_{NM})) \\ & \text{subject to } \mathbf{g}_{ij}(\bar{\mathbf{x}}_{ij}) \leq \mathbf{0}, \mathbf{h}_{ij}(\bar{\mathbf{x}}_{ij}) = \mathbf{0} \\ & \text{where } \bar{\mathbf{x}}_{ij} = [\mathbf{x}_{ij}, \mathbf{r}_{ij}, \mathbf{t}_{(i+1)k_1}, \dots, \mathbf{t}_{(i+1)k_{c_{ij}}}], \mathbf{c} = [\mathbf{c}_{22}, \dots, \mathbf{c}_{NM}] \end{aligned} \quad (2)$$

In the above,  $\mathbf{x}_{ij}$  is the vector of local design variables for element  $j$  at level  $i$ ,  $\mathbf{t}_{ij}$  is the vector of target coupling variables for element  $j$  at level  $i$  passed from its parent at level  $(i-1)$ ,  $\mathbf{r}_{ij}$  is the vector of response coupling variables for element  $j$  at level  $i$  passed to its parent at level  $(i-1)$ ,  $\mathbf{c}_{ij} = \mathbf{t}_{ij} - \mathbf{r}_{ij}$  is the vector of consistency constraints between target and response coupling variables,  $f_{ij}$  is the local objective function for element  $j$  at level  $i$ ,  $\pi$  is the penalty function,  $\mathbf{g}_{ij}$  is the vector of inequality constraints for element  $j$  at level  $i$ , and  $\mathbf{h}_{ij}$  is the vector of equality constraints for element  $j$  at level  $i$ . Ideally, the consistency constraints should evaluate to zero for an exact system solution; however, this is typically not feasible due to issues such as non-differentiability at the solution and unknown minimal parameter values [1]. Therefore, the consistency constraints are relaxed and inserted into some penalty function  $\pi(\mathbf{c})$  that requires a resultant value that is within some small tolerance before the algorithm is terminated. For this study, an augmented-Lagrangian (AL) penalty function was chosen, which resulted in the following general ATC-AL subproblem formulation for the  $i$ th level and the  $j$ th element [1]:

$$\begin{aligned} & \min_{\bar{\mathbf{x}}_{ij}} f_{ij}(\bar{\mathbf{x}}_{ij}) - \mathbf{v}_{ij}^T \mathbf{r}_{ij} + \sum_{k \in C_{ij}} \mathbf{v}_{(i+1)k}^T \mathbf{t}_{(i+1)k} + \left\| \mathbf{w}_{ij} \circ (\mathbf{t}_{ij} - \mathbf{r}_{ij}) \right\|_2^2 + \sum_{k \in C_{ij}} \left\| \mathbf{w}_{ij} \circ (\mathbf{t}_{(i+1)k} - \mathbf{r}_{(i+1)k}) \right\|_2^2 \\ & \text{subject to } \mathbf{g}_{ij}(\bar{\mathbf{x}}_{ij}) \leq \mathbf{0}, \mathbf{h}_{ij}(\bar{\mathbf{x}}_{ij}) = \mathbf{0} \\ & \text{where } \bar{\mathbf{x}}_{ij} = [\mathbf{x}_{ij}, \mathbf{r}_{ij}, \mathbf{t}_{(i+1)k_1}, \dots, \mathbf{t}_{(i+1)k_{c_{ij}}}] \end{aligned} \quad (3)$$

Here, the vectors  $\mathbf{v}$  and  $\mathbf{w}$  are weights corresponding to linear and quadratic terms in the AL penalty function, respectively. These decomposed problems are solved in an inner loop strategy where the weights remain constant. After performing an outer loop convergence check for each iteration  $K$ , the weights are updated according to the following scheme:

$$\begin{aligned} \mathbf{v}^{(K+1)} &= \mathbf{v}^{(K)} + 2\mathbf{w}^{(K)} \circ \mathbf{w}^{(K)} \circ \mathbf{c}^{(K)} \\ \mathbf{w}^{(K+1)} &= \beta \mathbf{w}^{(K)}, \text{ where } \beta \geq 1 \end{aligned} \quad (4)$$

The information flow for the general ATC-AL subproblem is illustrated in Figure 1.

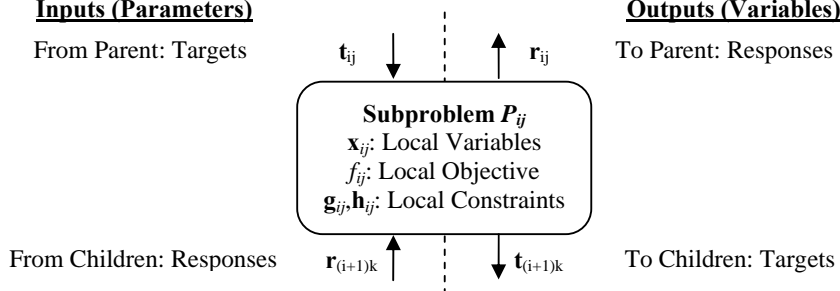


Figure 1: ATC Information Flow [1]

### 5. Reduced Representations of Vector-Valued Coupling Variables

This section describes the details of RBF ANN and POD representations, and how they are implemented in the current study.

#### 5.1. Radial-Basis Function Artificial Neural Networks

RBF ANN is a technique that develops a mapping to describe the functional relationship between sample input/output vector pairs  $\mathbf{y}_i = [y_1, y_2, \dots, y_p]^T$  and  $\mathbf{z}_i = [z_1, z_2, \dots, z_q]^T$  for all  $i = 1 \dots M$  samples such that the exact function  $\mathbf{z} = \mathbf{f}(\mathbf{y})$  can be approximated at any input vector  $\mathbf{y}_j$  in the sampling domain. This mapping is accomplished through a weighted, linear combination of RBFs:

$$\mathbf{z} = \mathbf{f}(\mathbf{y}) \approx \mathbf{g}(\mathbf{y}) = \sum_{k=1}^N \phi_{rbf,k}(\mathbf{y}) \omega_k \quad (5)$$

Here,  $\mathbf{g}(\mathbf{y})$  is the approximation to the exact function  $\mathbf{f}(\mathbf{y})$ ,  $\phi_{rbf,k}(\mathbf{y})$  is the  $k$ th RBF,  $N$  is the number of RBFs and neurons, and  $\omega_k$  is the  $k$ th weight vector. Although many different types of RBFs can be used, the one most commonly employed for these neural networks is the Gaussian density function:

$$\phi_{rbf,k}(\mathbf{y}) = (2\pi)^{-p/2} |\Sigma_k|^{-\frac{1}{2}} e^{-\frac{1}{2} (\mathbf{y} - \boldsymbol{\gamma}_k)^T \Sigma_k^{-1} (\mathbf{y} - \boldsymbol{\gamma}_k)} \quad (6)$$

In the above,  $p$  denotes the dimensionality of the input,  $\Sigma$  denotes the covariance matrix corresponding to the nodes, and  $\boldsymbol{\gamma}$  denotes the center of the basis function. Using  $M$  sampling pairs, the neural network is designed (or “trained”) by determining  $\omega_k$  associated with each RBF that minimizes the error between the exact function and its approximation in a least-squares sense:

$$\|\mathbf{f} - \mathbf{g}\| = \sqrt{\sum_{i=1}^M (\mathbf{z}_i - \mathbf{g}(\mathbf{y}_i))^2} \quad (7)$$

Because the neural network design requires  $k$  weight vectors, each of dimension  $q$ , the total number of representation variables would be  $kq \geq q$ . This contradicts the motivation for use as a reduced representation. However, the dimensionality of  $\mathbf{y}$  is usually significantly less than that of  $\mathbf{z}$  ( $p \ll q$ ); therefore, the elements within the input vector can be used as reduced representation variables.

In the EV design study [2], three RBF ANN were designed to relate the input vectors, which consisted of motor design variables, to the output vectors, which in turn consisted of VVCVs associated with maximum and minimum motor torque curves as well as power loss maps:

$$\mathbf{z}_{\max} \approx \mathbf{g}_{\max}(\mathbf{y}), \mathbf{z}_{\min} \approx \mathbf{g}_{\min}(\mathbf{y}), \mathbf{z}_{\text{pLoss}} \approx \mathbf{g}_{\text{pLoss}}(\mathbf{y}) \quad (8)$$

The motor design variables were based on the EV powertrain system model developed by Allison [23] and included stack length  $\ell_s$ , rotor radius  $r_m$ , rotor resistance  $R_r$ , and number of turns per stator coil  $n_c$  ( $p = 4$ ):

$$\mathbf{y} = [\ell_s, r_m, R_r, n_c]^T \quad (9)$$

The VVCVs, in turn, were determined by processing the motor design variables in a motor simulation within the powertrain model. Each VVCV associated with the torque curves contained  $q_{\max} = q_{\min} = 21$  values, whereas the VVCV associated with the power loss map contained  $q_{\text{pLoss}} = 861$  values:

$$\begin{aligned} \mathbf{z}_{\max} &= [z_{\max,1}, z_{\max,2}, \dots, z_{\max,q_{\max}}]^T \\ \mathbf{z}_{\min} &= [z_{\min,1}, z_{\min,2}, \dots, z_{\min,q_{\min}}]^T \\ \mathbf{z}_{\text{pLoss}} &= [z_{\text{pLoss},1}, z_{\text{pLoss},2}, \dots, z_{\text{pLoss},q_{\text{pLoss}}}]^T \end{aligned} \quad (10)$$

The set of training input/output vector pairs was generated by performing a six-level, full-factorial design of experiments (DOE), resulting in a total of  $M = 1296$  samples. Using these training vector pairs, the neural

networks were developed in MATLAB® with the *newrb* function, which enforces zero approximation error on all training vectors. Note that the training vectors were normalized to enhance the design and subsequent performance of the neural networks. Based on inspection, it can be seen that implementing RBF ANN under the strict condition that  $p \ll q$  significantly reduces the combined dimensionality of the VVCVs from  $Q = q_{max} + q_{min} + q_{pLoss} = 903$  to  $Q = p = 4$ .

### 5.2. Proper Orthogonal Decomposition

POD is a method commonly used to simplify the analysis and computation of dynamic systems in engineering applications. Specifically, it reduces the state-space representation of dynamic systems according to the following mapping [18]:

$$\mathbf{z}(t) \approx \mathbf{V}_p \mathbf{z}_r(t) \quad (11)$$

In the above,  $\mathbf{z}(t)$  is the original state vector of dimension  $q$ ,  $\mathbf{z}_r(t)$  is the reduced state vector of dimension  $p \ll q$ , and  $\mathbf{V}_p$  is a matrix containing the  $p$  most energetic basis functions used to construct the approximation of the original state vector. Without any loss of generality, the VVCVs in this study can be thought of as state vectors, and therefore the mapping in Eq. (11) can be modified as

$$\mathbf{z} \approx \mathbf{V}_p \mathbf{z}_r, \quad (12)$$

where  $\mathbf{z}$  is the original VVCV of dimension  $q$ ,  $\mathbf{z}_r$  is the reduced representation of dimension  $p \ll q$ , and  $\mathbf{V}_p$  is a matrix containing the  $p$  most energetic basis functions used to construct the approximation of the original VVCV. This matrix expression is developed through the “method of snapshots” [20], which begins by using  $M$  samples of the VVCV to form a correlation matrix  $\mathbf{R}$ :

$$\mathbf{R} = \mathbf{Z}^T \mathbf{Z} \quad (13)$$

Here,  $\mathbf{Z}$  is a  $(q \times M)$  matrix containing all samples of the original VVCV. The next step is to solve the eigenvalue problem associated with the correlation matrix,

$$\mathbf{R}\mathbf{a} = \boldsymbol{\lambda}\mathbf{a} \quad (14)$$

where  $\mathbf{a}$  represents the matrix of eigenvectors and  $\boldsymbol{\lambda}$  represents the diagonal matrix of associated eigenvalues, both of dimension  $(M \times M)$ . The basis functions used to construct the approximation of the VVCV are formulated according to

$$\mathbf{V} = \mathbf{Z}\mathbf{a} \quad (15)$$

where  $\mathbf{V}$  is the basis function matrix of dimension  $(q \times M)$ . This captures the essence of the “method of snapshots”, which states that each basis function is a linear combination of the  $M$  sample vectors [18]. Also, the basis functions in  $\mathbf{V}$  are arranged based on the magnitude of their associated eigenvalues:

$$\mathbf{V} = [\mathbf{v}_1, \mathbf{v}_2, \dots, \mathbf{v}_M], \quad \lambda_1 > \lambda_2 > \dots > \lambda_M \quad (16)$$

The eigenvalues are indicators of the energy of a given basis function; that is, large eigenvalues are associated with high-energy basis functions, whereas small eigenvalues are associated with low-energy basis functions. In determining the reduced basis function matrix  $\mathbf{V}_p$  from  $\mathbf{V}$ , it is suggested to choose the first  $p$  eigenvalues that achieve a relative energy ratio of 0.99 [24]. Although this approach generally ensures that the error in reconstructing the sample vectors from the reduced vectors is small, it does not directly quantify the approximation error. Furthermore, because the representation accuracies of both POD and RBF ANN are compared to one another, it is imperative that similar approaches be used in assessing in-sample accuracy for setting modeling parameters. Therefore, the following heuristic [2], which is based on average, root-mean-square (RMS) error, has been devised to determine the  $p$  most energetic basis functions:

$$\min_p RMS_{avg} = \sqrt{\frac{\sum_{i=1}^M \frac{(\mathbf{z}_i - \mathbf{V}_p \mathbf{z}_{r,i})^2}{q}}{M}} \quad (17)$$

This states that the most energetic basis functions are found by minimizing the average RMS error between the VVCV and its POD approximation across all samples. While this approach does not guarantee zero approximation error on the sample vectors as in the *newrb* function for RBF ANN, it does use the same concept to enforce the highest accuracy POD approximation possible.

For the current study, three POD representations were developed to approximate the VVCVs in Eq. (10):

$$\mathbf{z}_{max} \approx \mathbf{V}_{p,max} \mathbf{z}_{r,max}, \quad \mathbf{z}_{min} \approx \mathbf{V}_{p,min} \mathbf{z}_{r,min}, \quad \mathbf{z}_{pLoss} \approx \mathbf{V}_{p,pLoss} \mathbf{z}_{r,pLoss} \quad (18)$$

The sample vectors used in constructing these expressions were identical to those used in the RBF ANN. After applying Eqs. (13)-(17), it was found that the dimensions of the reduced representation vectors associated with the torque curves were  $p_{max} = p_{min} = 9$ , while the dimension of the reduced representation vector associated with the

power loss map was  $p_{pLoss} = 14$ . Implementing POD significantly reduces the individual dimensionality of each VVCV and the combined dimensionality;  $Q$  is reduced from 903 to  $Q = p_{max} + p_{min} + p_{pLoss} = 32$ .

## 6. Electric Vehicle Powertrain Model

The electric vehicle (EV) simulation model considered here was based on Allison [23]. A general plan view of the vehicle can be seen in Figure 2. The model is for a two-passenger, mini-compact vehicle designed for urban driving with some highway speed capability. This classification is evident by its overall dimensions, which includes a wheelbase of  $L = 1.80$  m and a track width of  $W = 1.27$  m. The vehicle is powered by a lithium-ion battery, which can vary in length, width, and longitudinal location relative to the vehicle front end such that it lies within the dashed region defined by length  $\ell_{max} = 1.05$  m and width  $b_{wmax} = 1.20$  m. Two electric traction motors drive the rear wheels through a synchronous belt drive system and have been mounted at the pivots on the rear suspension trailing arms in an effort to minimize the unsprung mass in the system. A MacPherson strut configuration was used for the front suspension, and finally, low rolling resistance P145/70R12 tires were used to minimize energy consumption.

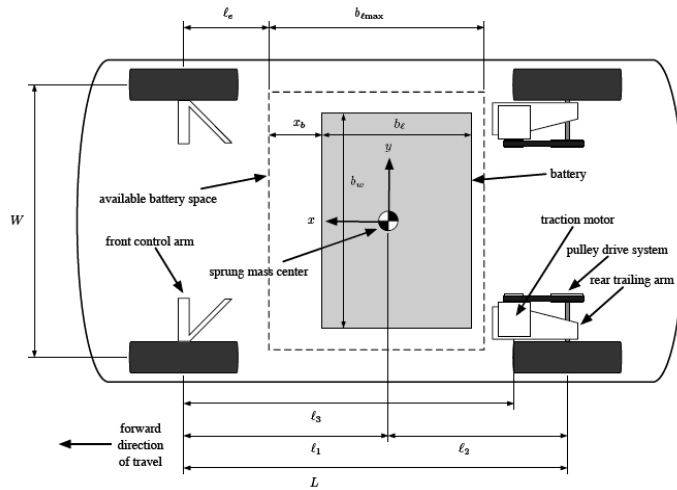


Figure 2: General Plan View of Electric Vehicle [23]

This study explores powertrain design exclusively, and so several modifications [2] were made to the analysis models within the simulation. The structural analysis model, for example, was held fixed and thus excluded from the design problem. The powertrain analysis model was decomposed into three separate entities, the electric motor, battery size, and vehicle analysis models. Any remaining input/output variables from the original powertrain analysis model (e.g., suspension variables) that were unaccounted for during decomposition were treated as parameters. The new analysis models are defined as [2]:

$$\begin{aligned} [\mathbf{z}_{\max}, \mathbf{z}_{\min}, \mathbf{z}_{pLoss}, J_r, \omega_{\max}] &= \mathbf{f}_{em}(\ell_s, r_m, R_r, n_c) \\ [b_m, b_w, b_\ell] &= \mathbf{f}_{bs}(B_I, B_W, B_L) \\ [m_s, \ell_1, h, I_y, I_z, g_{p1}, g_{p2}] &= \mathbf{f}_{mp}(b_m, b_w, b_\ell, x_b) \\ [mpg_e, t_{60}, \tau_v, \omega_v, R, P_V, C_b] &= \mathbf{f}_v(m_s, \ell_1, h, I_y, p_r, \mathbf{z}_{\max}, \mathbf{z}_{\min}, \mathbf{z}_{pLoss}, J_r, \omega_{\max}, B_I, B_W, B_L, b_m) \end{aligned} \quad (19)$$

The functions  $\mathbf{f}_{em}$ ,  $\mathbf{f}_{bs}$ ,  $\mathbf{f}_{mp}$ , and  $\mathbf{f}_v$  correspond to the electric motor, battery size, mass distribution and packaging, and vehicle analysis models, respectively. Table 1 provides definitions for the input/output variables of each function, and Figure 3 illustrates the relationships among the analysis models. Note that the dashed boxes in the figure indicate the problem decomposition for design optimization, which considers the interaction between the vehicle system and the motor subsystem.

Table 1: Definitions of Input/Output Variables to Analysis Models

Variable	Definition	Variable	Definition
$\ell_s$	Motor stack length (m)	$m_s$	Sprung mass (kg)
$r_m$	Rotor radius (m)	$l_1$	Center of mass longitudinal position (m)
$R_r$	Rotor resistance ( $\Omega$ )	$h$	Center of mass vertical position (m)
$n_c$	Number of turns per stator coil	$I_y$	Pitch moment of inertia ( $\text{kg}\cdot\text{m}^2$ )
$z_{\max}$	VVCV associated with max torque curve	$I_z$	Yaw moment of inertia ( $\text{kg}\cdot\text{m}^2$ )
$z_{\min}$	VVCV associated with min torque curve	$g_{p1}$	1 <sup>st</sup> battery packaging constraint
$z_{\text{pLoss}}$	VVCV associated with power loss map	$g_{p2}$	2 <sup>nd</sup> battery packaging constraint
$J_r$	Rotor moment of inertia ( $\text{kg}\cdot\text{m}^2$ )	$p_r$	Pulley speed ratio
$\omega_{\max}$	Max motor speed (rad/s)	$\text{mpg}_e$	Gasoline-equivalent fuel economy
$B_I$	Battery electrode thickness scale	$t_{60}$	0-60 time (s)
$B_W$	Battery cell width scale	$\tau_V$	Torque violation constraint
$B_L$	Number of cell windings	$\omega_V$	Speed violation constraint
$b_m$	Battery mass (kg)	$R$	Vehicle range (mi)
$b_w$	Battery width (m)	$P_V$	Power violation constraint
$b_\ell$	Battery length (m)	$C_b$	Battery capacity constraint (A-h)
$x_b$	Battery compartment clearance (m)		

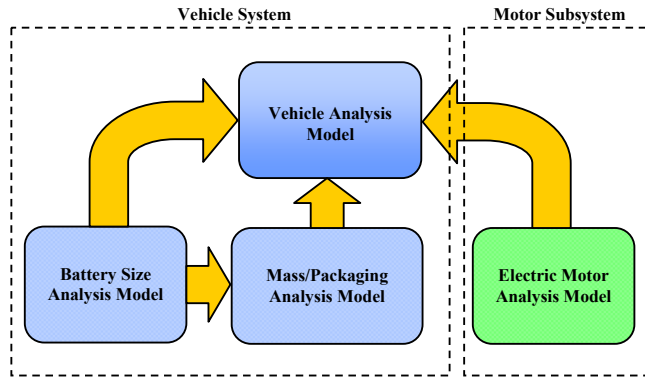


Figure 3: Analysis Model Relationships

## 7. ATC Problem Formulation and Results

The general ATC problem formulation for the EV powertrain system consists of a two-level hierarchical decomposition based on Eq. (3). The vehicle system described in Figure 3 is the top-level subproblem and the motor subsystem described in the same figure is the bottom-level subproblem. The vehicle system objective is to maximize gasoline-equivalent fuel economy while minimizing the AL penalty function, whereas the motor subsystem objective is to minimize the AL penalty function exclusively. Although both subproblems are subject to decision variable bound constraints, only the top level contains inequality constraints based on packaging, performance, motor feasibility, power consumption, and battery capacity.

Applying Eq. (3) directly, the vehicle subproblem  $P_{11}$  (excluding bound constraints) is:

$$\begin{aligned}
 & \min_{\bar{\mathbf{x}}_{11}} -\text{mpg}_e(\bar{\mathbf{x}}_{11}) + \mathbf{v}_{21}(\mathbf{t}_{21} - \mathbf{r}_{21}) + \|\mathbf{w}_{21} \circ (\mathbf{t}_{21} - \mathbf{r}_{21})\|_2^2 \\
 & \text{subject to } g_1(\bar{\mathbf{x}}_{11}) = b_w(\bar{\mathbf{x}}_{11}) - b_{w\max} \leq 0 \quad g_5(\bar{\mathbf{x}}_{11}) = \omega_V(\bar{\mathbf{x}}_{11}) \leq 0 \\
 & \quad g_2(\bar{\mathbf{x}}_{11}) = b_l(\bar{\mathbf{x}}_{11}) + x_b - b_{\ell\max} \leq 0 \quad g_6(\bar{\mathbf{x}}_{11}) = R_{\min} - R(\bar{\mathbf{x}}_{11}) \leq 0 \\
 & \quad g_3(\bar{\mathbf{x}}_{11}) = t_{60}(\bar{\mathbf{x}}_{11}) - t_{60\max} \leq 0 \quad g_7(\bar{\mathbf{x}}_{11}) = P_V(\bar{\mathbf{x}}_{11}) \leq 0 \\
 & \quad g_4(\bar{\mathbf{x}}_{11}) = \tau_V(\bar{\mathbf{x}}_{11}) \leq 0 \quad g_8(\bar{\mathbf{x}}_{11}) = C_b(\bar{\mathbf{x}}_{11}) - C_{b\max} \leq 0
 \end{aligned} \tag{20}$$

where  $\bar{\mathbf{x}}_{11} = [B_I, B_W, B_L, x_b, p_r, \mathbf{z}_{comb,r}^T, J_r^T, \omega_{\max}^T]$   
 $\mathbf{t}_{21} = [\mathbf{z}_{comb}^T, J_r^T, \omega_{\max}^T], \quad \mathbf{z}_{comb}^T = f(\mathbf{z}_{comb,r}^T), \quad \mathbf{r}_{21} = [\mathbf{z}_{comb}^R, J_r^R, \omega_{\max}^R]$

In the above,  $g_1 = g_{p1}$  and  $g_2 = g_{p2}$  are battery packaging constraints,  $g_3$  is a performance (0-60 time) constraint,  $g_4$  and  $g_5$  are motor feasibility constraints,  $g_6$  is a vehicle range constraint,  $g_7$  is a power violation constraint, and  $g_8$  is

a battery capacity constraint [23]. It should be noted that  $\mathbf{z}_{\text{comb}}$  and  $\mathbf{z}_{\text{comb},r}$  refer to the original vector of combined VVCVs and the combined vector of reduced representation variables, respectively. Also, observe that the superscripts  $T$  and  $R$  denote target and response versions of the same coupling variable, respectively. Similarly, the motor subproblem  $P_{21}$  (excluding bound constraints) can be formally described as:

$$\begin{aligned} \min_{\bar{\mathbf{x}}_{21}} \quad & \mathbf{v}_{11}(\mathbf{t}_{11} - \mathbf{r}_{11}) + \|\mathbf{w}_{11} \circ (\mathbf{t}_{11} - \mathbf{r}_{11})\|_2^2 \\ \text{where} \quad & \bar{\mathbf{x}}_{21} = [\ell_s, r_m, R_r, n_c] \\ & \mathbf{t}_{11} = [\mathbf{z}_{\text{comb}}^T, J_r^T, \omega_{\max}^T], \quad \mathbf{r}_{11} = [\mathbf{z}_{\text{comb}}^R, J_r^R, \omega_{\max}^R] = f(\bar{\mathbf{x}}_{21}) \end{aligned} \quad (21)$$

The problem formulation shown in Eqs. (20)-(21) has been solved by implementing RBF ANN and POD separately as reduced representations of the VVCVs associated with motor torque boundary curves and a power loss map. Due to the presence of non-smoothness in the powertrain model, a non-gradient-based optimization algorithm known as NOMADm [25] was used. The default settings for this MATLAB®-based optimizer were adequate for the current study. Finally, in optimizing the powertrain system for each reduced representation, identical starting points were used.

### 7.1 Optimization Results using RBF ANN

The optimization results using RBF ANN as a reduced representation technique are displayed in Tables 2-4. The algorithm successfully converged after two ATC iterations and resulted in a system solution that was consistent between both subproblems with the exception of the consistency constraint on  $J_r$ . In the vehicle subproblem, the bound constraint on  $\omega_{\max}^T$  was active and constraints  $g_3$  and  $g_6$  were also active. This behavior was expected as maximizing fuel economy directly compromises vehicle performance and range. In the motor subproblem, however, none of the bound constraints were active. Under these design conditions, the EV achieved a gasoline-equivalent fuel economy of approximately 200 mpg using the optimal motor map illustrated in Figure 4.

Table 2: Optimal Consistency Constraint Vector and Penalty Weights

Consistency Constraint	$\mathbf{c}_{\text{opt}}$	$\mathbf{v}_{\text{opt}}$	$\mathbf{w}_{\text{opt}}$
$c_{z,\max}$	0.60	1.15	1.5
$c_{z,\min}$	0.50	1	1.5
$c_{z,pLoss}$	0.80	1.65	1.5
$c_{J_r}$	-0.15	-0.30	1.5
$c_{\omega,\max}$	-0.05	-0.10	1.5

Table 3: Optimal Decision Vector for Vehicle Subproblem

Vehicle Subproblem, $P_{11}$											
Variable	$B_I$	$B_W$	$B_L$	$x_b$	$p_r$	$\ell_s^T$	$r_m^T$	$R_r^T$	$n_c^T$	$J_r^T$	$\omega_{\max}^T$
Value	0.75	1	20	0.10	2	0.13	0.12	0.09	11	0.20	755
Activity	--	--	--	--	--	--	--	--	--	--	X

Table 4: Optimal Decision Vector for Motor Subproblem

Motor Subproblem, $P_{21}$			
Variable	$\ell_s^R$	$r_m^R$	$R_r^R$
Value	0.12	0.13	0.06
Activity	--	--	--

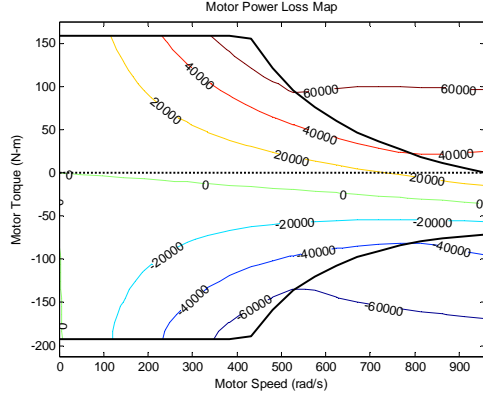


Figure 4: Optimal Motor Power Loss Map

### 7.2 Optimization Results using POD

In implementing POD as a reduced representation technique during optimization, the algorithm failed due to a powertrain simulation crash. Figures 5-6 provide some insight to the cause of this failure. In particular, Figure 5 indicates that the POD approximation of the motor map at the failed design point was faulty; that is, it did not exhibit behavior similar to the motor map shown in Figure 4. Figure 6 builds upon this information by revealing that the failed design point was not physically realizable. Specifically, the original assumption that the POD design space was defined by simple bound constraints was incorrect; instead, nonlinear constraints characterized this design space. It should be noted that Figure 6 only captures one of these constraints graphically; in reality, there could be many other interactions among the reduced representation variables, leading to possibly hundreds of other constraints. The identification and formulation of these nonlinear constraints is outside the scope of this study and is proposed as a topic for future work.

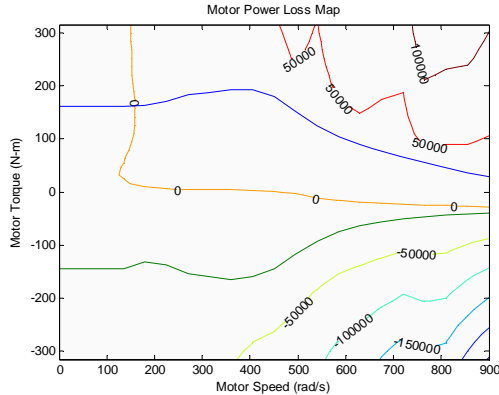


Figure 5: Motor Power Loss Map using POD

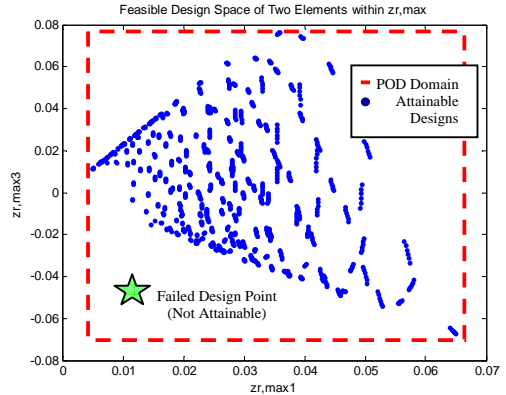


Figure 6: Design Space of Two POD Variables

### 8. Efficiency and Accuracy Assessment

The efficiency of each reduced representation in terms of their impact on decision vector dimensionality is evident upon inspection of their respective vehicle subproblems. When using RBF ANN,  $x_{11}$  contained 5 local design variables, 4 reduced representation variables, and 2 additional coupling variables. This yielded a decision vector dimensionality of 11. The same number of local design and coupling variables were present when using POD; however, 32 reduced representation variables were also used, yielding a decision vector dimensionality of 39. This indicates that RBF ANN performed better in terms of efficiency.

The accuracy of each reduced representation was quantified by using a comparison tool known as AVASIM [26], which characterizes the local and global error between exact and approximation models through  $\ell_1$ -norms. From these norms, error indices are constructed such that nonnegative values denote valid approximation models with accuracy levels between 0 and 1, and all negative values denote invalid approximation models. Note that

validity is defined by approximations that lie within some preset threshold value; therefore, a value of 0 indicates that an approximation is at the threshold and valid, whereas a value of 1 indicates that an approximation is completely accurate. AVASIM was applied with a 3% tolerance to measure the accuracy in the torque curves and power loss maps produced by RBF ANN and POD. Tables 5-6 show the results of these calculations and indicate that RBF ANN performed better in terms of accuracy.

Table 5: AVASIM Results for RBF ANN

Index	$Z_{\max}$	$Z_{\min}$	$Z_{pLoss}$
$E_{local}$	0.91	0.94	-2.54
$E_{global}$	0.93	0.94	0.91
$E_{combined}$	0.92	0.94	-0.82

Table 6: AVASIM Results for POD

Index	$Z_{\max}$	$Z_{\min}$	$Z_{pLoss}$
$E_{local}$	0.44	0.83	-9.60
$E_{global}$	0.77	0.84	0.37
$E_{combined}$	0.61	0.84	-4.61

## 9. Conclusions and Future Work

Based on these initial results, one may conclude that RBF ANN is the best reduced representation technique to use for VVCVs present in ATC problem formulations. The use of this representation was able to produce an optimal solution with low decision vector dimensionality and reasonable accuracy of the motor torque boundary curves. A key issue in using methods such as POD successfully is properly identifying and formulating the constraints defining the design space of their representation variables. Like any optimization problem, there may be nonlinear constraints that characterize the design space in addition to simple bound constraints. The challenge in formulating constraints for these methods is that the reduced representation variables often have no physical meaning, leaving their interactions to be described purely in terms of advanced mathematical techniques. Therefore, implementation of POD in the current context requires further research.

An important observation can be made in inspecting Eqs. (20)-(21) for the RBF ANN implementation. The decision vector  $\mathbf{x}_{2|1}$  is identical to the reduced representation variables in  $\mathbf{x}_{1|1}$ . This presents both a theoretical and practical problem in that the key motivation in using the ATC formulation is to partition the original system design problem into subproblems that are unique with the exception of coupling variables. If the set of decision variables for a given subproblem only include coupling variables, then such a subproblem is not truly unique and should be incorporated into the larger system problem. This implies that an all-in-one formulation could be used to solve the problem rather than ATC. Therefore, a meaningful use of RBF ANN as the reduced representation of VVCVs in an ATC implementation would be, for example, when local objectives are present in the subproblems. Otherwise, methods that employ coupling variables that are distinct from design variables in each subproblem, such as POD, would need to be considered.

Finally, it should be observed that the power loss map approximations for both RBF ANN and POD were deemed invalid based on the AVASIM metric. Although the relatively tight error tolerance might have contributed to this lack of validity, the most likely cause was an insufficient sample size based on preliminary investigation. Further exploration into this issue would be desirable.

## 10. Acknowledgements

This work was partially supported by the Automotive Research Center, which is a U.S. Army Center of Excellence at the University of Michigan, as well as the U.S. National GEM Consortium. This support is gratefully acknowledged.

## 11. References

- [1] Tossarams, S., Etman, L.F.P., Papalambros, P.Y., and Rooda, J.E., 2006, “An augmented Lagrangian relaxation for analytical target cascading using the alternating direction method of multipliers”, *Structural Multidisciplinary Optimization*, Vol. 31, pp. 176-189.
- [2] Alexander, M.J., “Analytical Target Cascading Optimization of an Electric Vehicle Powertrain System”, M.S. thesis, University of Michigan, 2008.
- [3] Sobieski, L. and Kroo, I., “Aircraft Design using Collaborative Optimization”, AIAA 34<sup>th</sup> Aerospace Sciences Meeting and Exhibit, Reno, NV, Jan. 15-18, 1996.
- [4] Wang, G.G., and Shan, S., “Review of Metamodeling Techniques in Support of Engineering Design Optimization”, *Journal of Mechanical Design*, Vol. 129, No. 4, pp. 371-380, 2007.
- [5] Bradie, B. *A Friendly Introduction to Numerical Analysis*. Pearson Prentice Hall, Upper Saddle River, NJ, 2006.
- [6] George, P. and Ogot, M. M., 2006, “A Compromise Experimental Design Method for Parametric Polynomial Response Surface Approximations”, *Journal of Applied Statistics*, 33:10, 1037 — 1050.
- [7] Draper, N.R. and Pukelsheim, F., “Polynomial Representations for Response Surface Modeling”, Technical Report, University of Wisconsin-Madison and University of Washington, 1997.

- [8] Box, G.E.P. and Hunter, J.S., 1957, "Multi-factor experimental designs for exploring response surfaces", *The Annals of Mathematical Statistics*, 28:195-241.
- [9] Sansone, G. and Hille, E. *Orthogonal Functions*. Dover Publications Inc, Mineola NY, Rev. English ed., 2004.
- [10] Glasbey, C.A. and Mardia, K.V., 1998, "A review of image-warping methods", *Journal of Applied Statistics*, 25(2):155–172.
- [11] Stegmann, M.B., "Image Warping", Technical Report, Informatics and Mathematical Modeling, Technical University of Denmark, 2001.
- [12] Kokkolaras, M., Louca, L.S., Delagrammatikas, G.J., Michelen, N.F., Filipi, Z.S., Papalambros, P.Y., Stein, J.L., and Assanis, D.N., 2004, "Simulation-based optimal design of heavy trucks by model-based decomposition: An extensive analytical target cascading case study", *Int. J. Heavy Vehicle Systems*, Vol. 11, Nos.3/4, pp. 402-431.
- [13] Ahmed, W., Hummels, D.M. and Musavi, M.T., "A Fast Orthogonal Search Algorithm for Radial-Basis Function Neural Networks", Technical Report, Department of Electrical and Computer Engineering, University of Maine.
- [14] "Training Feedforward and Radial-Basis Function Networks", *Neural Networks Documentation*, Wolfram Research.
- [15] "Proper Orthogonal Decomposition", Class Lecture Notes, Department of Electrical Engineering and Computer Science, Massachusetts Institute of Technology, 2004.
- [16] Model Order Reduction Wiki-Model order reduction site at MIT,  
[http://scripts.mit.edu/~mor/wiki/index.php?title=Model\\_Order\\_Reduction\\_Wiki](http://scripts.mit.edu/~mor/wiki/index.php?title=Model_Order_Reduction_Wiki), Accessed 7 May 2007.
- [17] Lucia, D.J., Beran, P.S., and Silva, W.A., 2003, "Reduced-order modeling: new approaches for computational physics", *Progress in Aerospace Sciences*, 40:51-117.
- [18] Ahmed N., Goldstein M.H. *Orthogonal transforms for digital signal processing*. Berlin: Springer, 1975.
- [19] Wilcox, Karen, "An Introduction to Model Reduction for Large-Scale Applications", Aerospace Computational Design Laboratory Seminar, MIT, September 23, 2005,  
[http://web.mit.edu/mor/papers/ADCL\\_Sept05.pdf](http://web.mit.edu/mor/papers/ADCL_Sept05.pdf), Accessed 12 May 2007.
- [20] Burkhardt, J., Du, Q., Gunzburger, M., and Lee, H.C., "Reduced order modeling of complex systems", Proceedings of NA03, Dundee, 2003.
- [21] Kim, H.-M., 2001. Target Cascading in Optimal System Design. Ph.D. Dissertation, Department of Mechanical Engineering, University of Michigan, Ann Arbor, Michigan, USA.
- [22] Kim, H. M., Michelena, N. F., Papalambros, P. Y., and Jiang, T., "Target Cascading in Optimal System Design". *ASME Journal of Mechanical Design*, Vol. 125, No. 3, 2003, pp. 474-480.
- [23] Allison, J., "Optimal Partitioning and Coordination Decisions in Decomposition-based Design Optimization", Ph.D. dissertation, University of Michigan, 2008.
- [24] Bui-Thanh, T., Damodaran, M., and Wilcox, K., "Aerodynamic Reconstruction and Inverse Design Using Proper Orthogonal Decomposition", *AIAA Journal*, Vol. 42, No. 8, pp. 1505-1516, 2004.
- [25] Abramson, M.A. *NOMADm Version 4.5 User's Guide*, January 2007.
- [26] Sendur, P., Stein, J.L., Louca, L.S., and Peng, H., "A Model Accuracy and Validation Algorithm", Proceedings of 2002 ASME International Mechanical Engineering Congress and Exposition, New Orleans, LA, November 17-22, 2002.